Comparison of cooling rates for hot carriers in GaAs/AlAs quantum wells based on macroscopic and microscopic phonon models

Jian-zhong Zhang*
National Laboratory for Superlattices and Microstructures, Institute of Semiconductors, Chinese Academy of Sciences, P.O. Box 912, Beijing 100083, People's Republic of China

Bang-fen Zhu
National Laboratory for Superlattices and Microstructures, Institute of Semiconductors, Chinese Academy of Sciences, P.O. Box 912, Beijing 100083, People's Republic of China
and Center for Advanced Study, Tsinghua University, Beijing 100084, People's Republic of China

Kun Huang
National Laboratory for Superlattices and Microstructures, Institute of Semiconductors, Chinese Academy of Sciences, P.O. Box 912, Beijing 100083, People's Republic of China

(Received 7 October 1998; revised manuscript received 15 December 1998)

By using three analytical phonon models in quantum wells—the slab model, the guided-mode model, and the improved version of the Huang-Zhu model [Phys. Rev. B **38**, 13 377 (1998)], —and the phonon modes in bulk, the energy-loss rates of hot carriers due to the Fröhlich potential scattering in GaAs/AlAs multiple quantum wells (MQW's) are calculated and compared to those obtained based on a microscopic dipole superlattice model. In the study, a special emphasis is put on the effects of the phonon models on the hot-carrier relaxation process when taking the hot-phonon effect into account. Our numerical results show that, the calculated energy-loss rates based on the slab model and on the improved Huang-Zhu model are almost the same when ignoring the hot-phonon effect; however, with the hot phonon effect considered, the calculated cooling rate as well as the hot phonon occupation number do depend upon the phonon models to be adopted. Out of the four analytical phonon models investigated, the improved Huang-Zhu model gives the results most close to the microscopic calculation, while the guided-mode model presents the poorest results. For hot electrons with a sheet density around $10^{12}/\mathrm{cm}^2$, the slab model has been found to overestimate the hot-phonon effect by more than 40% compared to the Huang-Zhu model, and about 75% compared to the microscopic calculation in which the phonon dispersion is fully included. Our calculation also indicates that Nash's improved version [J. Lumin. **44**, 315 (1989)] is necessary for evaluating the energy-loss rates in quantum wells of wider well width, because Huang-Zhu's original analytical formulas are only approximately orthogonal for optical phonons associated with small in-plane wave numbers. [S0163-1829(99)08919-5]

I. INTRODUCTION

In most optical experiments the incident photons usually create ''hot'' carriers; that is, the temperature characterizing the carrier distribution, T_c, is higher than the lattice temperature T_L. The hot carriers have to relax to the bottom of the energy band before radiative recombination occurs with significant probability. This energy dissipation process is governed by emitting phonons, in particular longitudinal-optical (LO) phonons via the Fröhlich interaction in polar semiconductors when $T_c \geqslant 45$ K.

When the density of the photoexcited carriers is moderate to high, a large number of LO phonons may be generated in the hot-carrier relaxation process. The generated optical phonons will decay into acoustic phonons via anharmonic interaction. Since the average lifetime of optical phonons through anharmonic decay is typically several picoseconds, e.g., about 7 ps in GaAs,[1] which is much longer than the Fröhlich scattering time, the LO-phonon modes emitted during the relaxation process may be accumulated, leading to an occupation number of these modes that is larger than the population at equilibrium. If we relate the phonon population to the temperature, these relevant phonons are hot. Since the electron–LO-phonon interaction depends on the phonon mode, each phonon mode will have its distinct temperature; in other words, the hot-phonon distribution is at nonequilibrium. The first experimental evidence of such hot phonons was obtained by Shah, Leite, and Scoll in 1970.[2]

The hot phonons result in a slower cooling rate for hot carriers of high density than estimated by a simple model,[3] because the probability of reabsorbing the hot phonons by carriers is greatly enhanced. The hot-phonon effect has been accepted as the main factor responsible for the reduced cooling rate of hot carriers with a sheet density as high as $10^{10}/\mathrm{cm}^2$–$10^{12}/\mathrm{cm}^2$, which is also supported by much theoretical research.[4–6]

The hot-phonon effect in the hot carrier relaxation in quantum wells has been extensively studied during the past decade. However, the Fröhlich interaction potential in bulk materials was often used in most previous theoretical calculations,[7,8] which will be referred to as the three-dimensional phonon model in this paper. In principle, to study hot-carrier relaxation in quantum wells, the phonon eigenmodes in such structures should be considered. In the

past several years several research groups have calculated and compared the electron Fröhlich scattering rates based on different analytical phonon models[9,10] as well as microscopic phonon models.[10,11] They found[9,10,12,13] that the total or average electron-phonon scattering rate in a quantum well was insensitive to the phonon basis set selected, as long as the set was orthogonal and complete. Thus it seems reasonable to evaluate the hot-carrier relaxation rate by using any proper phonon model.

The claim above should be treated with caution. First, there is no simple sum rule when all the phonon modes including the interface modes and bulklike modes are not degenerate. Usually, the interface phonons, which play an important role in the electron-phonon scattering, deviate significantly from the bulk LO-phonon frequency. Second, another prerequisite of the independent scattering rate requires the orthogonality and completeness of the phonon basis set. The orthogonality and completeness of a basis set is defined by the differential equation, the spatial region, and the boundary condition. Compared with the easily verified orthogonality, the completeness of these bases, or the feasibility of the one-to-one transformation between different phonon basis sets, has only been verified numerically by using a sufficiently large number of basis functions.[9] But, in reality, the number of branches of the LO bulklike modes involved in the scattering is restricted to the number of monolayers in a well. The completeness of the basis, which spans a Hilbert space of infinite dimension, does not always guarantee the equivalence between two sets of phonon modes which are finite for an given parallel wave vector, in particular for an ultrathin quantum well. Last and most importantly, all the above considerations are based on an equilibrium phonon distribution; when the hot-phonon effect on the hot-carrier relaxation process must be taken into account, phonon modes are at nonequilibrium, and some modes will play a more important role than others. Thus, as speculated in Ref. 9, it is necessary to use the correct normal modes of the system to evaluate the energy-loss rate (ELR).

In the late 1980s, three analytic optical-phonon models, namely, (1) the dielectric continuum model, known as the slab model in some of its applications to the quantum wells,[14] (2) the guided-mode, or mechanical model,[15,16] and (3) the Huang-Zhu model[17] have been proposed to describe the polar optical vibration and the associated Fröhlich interaction potentials in quantum wells. The three analytic optical-phonon models predict quite different optical-phonon modes and potential functions based on different boundary conditions.

According to the dielectric continuum model, the polar vibration modes in semiconductor quantum wells are divided into confined (i.e., bulklike) modes and interface modes. The bulklike modes in the slab model obey the electrostatic boundary condition; that is, the electrostatic potential of the modes vanishes at the interfaces. On the other hand, the optical-phonon modes in the guided-mode model satisfy the mechanical boundary condition, i.e., the optical displacements have nodes at the interfaces. Based on their microscopic calculation from a dipole superlattice model,[18,19] which is compatible with the dielectric continuum model and will be referred to as the microscopic dipole superlattice model in this paper,[20] Huang and Zhu presented a set of analytical formulas and proposed a double boundary condition for the bulklike modes, in which both the electrostatic potential and the optical displacement vanish at the interfaces. However the interface modes in Huang-Zhu model are identical to that in the dielectric continuum model. In fact, the Huang-Zhu model is essentially the dielectric continuum model taking account of phonon dispersion and the double boundary condition.

In the early 1990s, experimental and theoretical investigations devoted to comparing these three analytic optical-phonon models in quantum wells was one of hot topics in the physics of semiconductors.[21–24,10] Since Tsen *et al.*[21] pointed out that their experimental data were in excellent agreement with the Huang-Zhu model, this model has obtained wide acceptance. However, as indicated in their original paper, the Huang-Zhu analytic expressions are orthogonal for phonons with an in-plane wave number less than or comparable with π/W_0 (W_0 is the well width), beyond which the orthogonality of the modes as well as their agreement with the microscopic calculation deteriorate.[17] Thus an improved version of the analytical formulas is required, and was given by Nash,[9,25] which will be referred to as the improved Huang-Zhu formulas in this paper.

Recently, by using the microscopic phonon model, the present authors performed a numerical calculation on hot-carrier relaxation dynamics in GaAs/AlAs multiple quantum wells (MQW's) in which the hot-phonon effect was taken into account.[26,27] By using the microscopic phonon model, the relationship between the hot-phonon effects and the effects due to the dimensionality, the carrier density, the phonon dispersion, and the hot-carrier temperature is presented. However, the full microscopic calculation on the ELR of hot carriers including the hot phonon effect is indeed very difficult work. As the analytical phonon models are convenient for practical usage, people naturally want to know whether the different phonon models affect the ELR of hot carriers, and, if so, what is the quantitative discrepancy between ELR's calculated with various analytic phonon models and those calculated by the microscopic phonon model. In particular, it is of interest to know the macroscopic model by which the ELR most close to the microscopic results can be obtained when including the hot-phonon effect. In addition, it is not easy for the microscopic phonon model to single out the contribution from certain phonon modes in the carrier relaxation process. Thus, in order to understand behaviors of different orders of confined modes and various interface modes in the coupled carrier-phonon system, it is also necessary to calculate the cooling rate of hot carriers by using analytical phonon models. For these purposes, in this paper, we intend to present a quantitative comparison among the ELR's of hot carriers in GaAs/AlAs MQW's calculated based on the microscopic phonon model and various macroscopic models, including three analytical phonon models in quantum wells as well as the three-dimensional phonon model, in which an emphasis is put on the phonon model effect on the ELR's when the hot-phonon effect is taken into account. Although the inadequacy within the guided-mode model has been admitted by the proponents of the model,[28] which was widely adopted and is still used by researchers unfamiliar with the debate on phonon models in quantum wells, we shall choose the guided-mode model as one of

models in examining the phonon model effect on ELR's of hot carriers.

This paper is organized as follows. In Sec. II, the electron–optical-phonon interactions in MQW's are illustrated for various phonon models. The electronic structures used in our calculation are described in Sec. III. Then the formalism for calculating the hot-phonon population and the carrier's ELR is given in Sec. IV. Numerical results on the hot-carrier relaxation in MQW's evaluated based on different phonon models are presented in Sec. V, where a critical comparison among these macroscopic models are performed and discussed and judged by the ELR's calculated with the microscopic model. Finally, in Sec. VI our conclusions are drawn.

II. ELECTRON-OPTICAL-PHONON INTERACTIONS IN QW's

A. Confined modes

The electron-confined-phonon Fröhlich interaction Hamiltonian in multiple quantum wells can be formally written as

$$H_{eb}(\vec{r}) = \gamma V^{-1/2}\omega_{LO}^{-1/2}\sum_{l}\sum_{\vec{q},n} I_n^{-1/2}(q_{||}) \times \Phi_n(z_l)e^{i\vec{q}_{||}\cdot\vec{r}_{||}+iq_z ld}[\hat{a}_{n,\vec{q}}+\hat{a}^{+}_{n,-\vec{q}}], \quad (1)$$

where the subscript eb denotes the electron–bulklike-phonon interaction, d is the period of the MQW's, V is the normalization volume, $\hat{a}_{n,\vec{q}}$, and $\hat{a}^{+}_{n,\vec{q}}$ are the annihilation and the creation operators for the phonon mode of $(n,\vec{q})$, respectively, in which n denotes the LO mode order index, and $\vec{q}=(\vec{q}_{||},q_z)$ is the phonon wave vector. Φ_n depicts the potential function for the nth branch of LO modes, which, being the analytic confined modes, is assumed to be independent of the phonon wave number. z_l represents $z-ld$, which, for the confined modes, is confined to the region of $|z_l| \leqslant W/2$, where the effective well width for the phonon modes $W=W_0+a_0$ (a_0 is the thickness of one monolayer).[29] γ is a constant decided by

$$\gamma^2 = 2\pi e^2\hbar(\omega_{LO}^2-\omega_{TO}^2)/\epsilon_\infty, \quad (2)$$

where ω_{LO} and ω_{TO}, respectively, are the LO-phonon and transverse optical (TO)-phonon frequency at the Γ point, $-e$ is the electron charge, ϵ_∞ is the high-frequency dielectric constant, and $\hbar$ is the Plank constant. In Eq. (1), $I_n(q_{||})$ is a constant determined by the normalization condition for the optical displacement, namely,

$$I_n(q_{||}) = \frac{1}{d}\int_{-W/2}^{W/2}\left[q_{||}^2\Phi_n^2(z)+\left(\frac{\partial\Phi_n}{\partial z}\right)^2\right]dz. \quad (3)$$

In the slab model, the potential of the nth phonon mode is

$$\Phi_n(z) = \begin{cases}\cos(n\pi z/W), & n=1,3,5,\ldots\\ \sin(n\pi z/W), & n=2,4,6,\ldots,\end{cases} \quad (4)$$

which vanishes at the interfaces to meet the electrostatic boundary condition.

In the guided-mode model, the nth mode potential is

$$\Phi_n(z) = \begin{cases}\sin(n\pi z/W), & n=1,3,5,\ldots\\ \cos(n\pi z/W), & n=2,4,6,\ldots,\end{cases} \quad (5)$$

where the derivative of the potentials satisfy the mechanical boundary condition at the interfaces, that is, the optical displacement has nodes at $\pm W/2$.

In the Huang-Zhu model, both the phonon mode potential and the optical displacement vanish at the interfaces, and the nth potential is formulated as

$$\Phi_n(z) = \begin{cases}\sin(\mu_n\pi z/W)+C_n z/W, & n=3,5,7,\ldots\\ \cos(n\pi z/W)-(-1)^{n/2}, & n=2,4,6,\ldots,\end{cases} \quad (6)$$

where μ_n and C_n are constants to be determined by the double boundary conditions, so that $\sin(\mu_n\pi/2)=-C_n/2$ and $\cos(\mu_n\pi/2)=-C_n/\mu_n\pi$.

In the improved formulas for the Huang-Zhu model, the nth mode potential is written as follows:[9]

$$\Phi_n(z) = \begin{cases}\cos(\mu_{nq}\pi z/W)+D_{nq}\cosh(q_{||}z), & n=2,4,6,\ldots\\ \sin(\mu_{nq}\pi z/W)+D_{nq}\sinh(q_{||}z), & n=3,5,7,\ldots.\end{cases} \quad (7)$$

This set of mode potential corresponds to an orthogonal basis set for the optical-phonon modes with arbitrary $q_{||}$. The constants μ_{nq} and D_{nq} in Eq. (7) are determined by the double boundary boundary conditions; that is, for odd n,

$$\tan\left(\frac{\mu_{nq}\pi}{2}\right) = \frac{\mu_{nq}\pi}{q_{||}W}\tanh\left(\frac{q_{||}W}{2}\right),$$
$$D_{nq} = -\sin\left(\frac{\mu_{nq}\pi}{2}\right)\Big/\sinh\left(\frac{q_{||}W}{2}\right); \quad (8)$$

and, for even n,

$$\tan\left(\frac{\mu_{nq}\pi}{2}\right) = -\frac{q_{||}W}{\mu_{nq}\pi}\tanh\left(\frac{q_{||}W}{2}\right),$$
$$D_{nq} = -\cos\left(\frac{\mu_{nq}\pi}{2}\right)\Big/\cosh\left(\frac{q_{||}W}{2}\right). \quad (9)$$

Notice that for MQW's with a well width of M monolayers, the maximum value of n in Eqs. (4)–(7) is $M-1$ for the slab and Huang-Zhu models, and is M for the guided model. Only when M is large can the bulklike modes together with the interface modes be approximately assumed to be complete.[30] If M is small, it is hard to map one basis set into another set with an acceptable accuracy.

B. Interface modes

According to the dielectric continuum model, in addition to the bulklike optical modes, there are four branches of interface modes in GaAs/AlAs MQW's. Unlike the bulklike modes, the interface modes exhibits a strong phonon dispersion. The frequencies of the interface modes are determined by the following equation, in which, for simplicity, an equal

thickness d_0 is taken for both the well and the barrier, i.e., $d=2d_0$:

$$\cos(q_z d)=\frac{\epsilon^2+\bar{\epsilon}^2}{2\epsilon\bar{\epsilon}}\sinh^2(q_{||}d_0)+\cosh^2(q_{||}d_0). \quad (10)$$

Here letters with or without an overbar are used to label physical quantities in the barrier or in the well layers, and ϵ and $\bar{\epsilon}$ are the corresponding dielectric functions, respectively:

$$\epsilon(\omega)=\epsilon_\infty\frac{\omega_{LO}^2-\omega^2}{\omega_{TO}^2-\omega^2}, \quad \bar{\epsilon}(\omega)=\bar{\epsilon}_\infty\frac{\bar{\omega}_{LO}^2-\omega^2}{\bar{\omega}_{TO}^2-\omega^2}. \quad (11)$$

The Hamiltonian for the electron–interface-phonon interaction can be written as

$$H_{ei}(\vec{r})=e\left(\frac{\pi}{2V}\right)^{1/2}\sum_l\sum_{\vec{q},n}\left(\frac{\hbar}{2\omega_n(\vec{q})}\right)^{1/2}\times I_{nq}J_{nq}(z_l)e^{i\vec{q}_{||}\cdot\vec{r}_{||}+iq_z ld}[\hat{a}_{n,\vec{q}}+\hat{a}^+_{n,-\vec{q}}], \quad (12)$$

where the subscript ei represents the electron–interface-phonon interaction, $n=1$, 2, 3, and 4 label four interface modes according to their frequency increase, and the function $J_{nq}(z)$ is defined as[31]

$$J_{nq}(z)=\begin{cases} Ae^{q_{||}z}-Be^{-q_{||}z}, & |z|\leq d_0/2 \\ \bar{A}e^{q_{||}(z-d_0)}-\bar{B}e^{-q_{||}(z-d_0)}, & d_0/2\leq z\leq d_0 \\ [\bar{A}e^{q_{||}(z+d_0)}-\bar{B}e^{-q_{||}(z+d_0)}]e^{iq_z d}, & -d_0\leq z\leq -d_0/2. \end{cases} \quad (13)$$

The coefficients A, B, $\bar{A}$, and $\bar{B}$ are defined as

$$A=(\bar{\epsilon}-\epsilon)e^{-q_{||}d_0/2}+(\bar{\epsilon}+\epsilon)e^{3q_{||}d_0/2}-2\bar{\epsilon}e^{-q_{||}d_0/2}e^{-iq_z d}, \quad (14a)$$

$$B=(\bar{\epsilon}-\epsilon)e^{q_{||}d_0/2}+(\bar{\epsilon}+\epsilon)e^{-3q_{||}d_0/2}-2\bar{\epsilon}e^{q_{||}d_0/2}e^{-iq_z d}, \quad (14b)$$

$$\bar{A}=(\bar{\epsilon}-\epsilon)e^{q_{||}d_0/2}-(\bar{\epsilon}+\epsilon)e^{-3q_{||}d_0/2}+2\epsilon e^{q_{||}d_0/2}e^{iq_z d}, \quad (14c)$$

$$\bar{B}=(\bar{\epsilon}-\epsilon)e^{-q_{||}d_0/2}-(\bar{\epsilon}+\epsilon)e^{3q_{||}d_0/2}+2\epsilon e^{-q_{||}d_0/2}e^{iq_z d}. \quad (14d)$$

Here I_{nq} is a normalization constant given by

$$I_{nq}=[1-\cos(q_z d)]^{-1/2}\{(\bar{\epsilon}-\epsilon)[\bar{\epsilon}S^2(\omega)-\epsilon\bar{S}^2(\omega)]\}^{-1/2}[q_{||}d_0/\sinh(q_{||}d)]^{1/2}/q_{||}, \quad (15)$$

where $S(\omega)$ and $\bar{S}(\omega)$ are written as

$$S(\omega)=\epsilon_\infty^{1/2}\frac{(\omega_{LO}^2-\omega_{TO}^2)^{1/2}}{\omega_{TO}^2-\omega^2}, \quad \bar{S}(\omega)=\bar{\epsilon}_\infty^{1/2}\frac{(\bar{\omega}_{LO}^2-\bar{\omega}_{TO}^2)^{1/2}}{\bar{\omega}_{TO}^2-\omega^2}. \quad (16)$$

When a pair of GaAs- or AlAs-like interface phonons are degenerate, the potential functions given above will be transformed into the linear combination of the degenerate functions according to the symmetry, which are not shown here for simplicity.

In the Huang-Zhu model, the mode $n=1$ is automatically excluded from the bulklike mode series. As indicated by Huang and Zhu,[17] the $n=1$ modes exhibit typical dispersion curves and potentials for the interface modes predicted by the dielectric continuum model. Thus the identical potential functions with the interface modes in the dielectric continuum model are taken in the Huang-Zhu model.

C. Microscopic LO-phonon mode potential

In Huang and Zhu's dipole superlattice model, the optical-phonon mode of the multiple quantum wells, $(n,\vec{q})$, is expressed as the linear superposition of the vibrational mode of the bulk dipole lattice, namely,

$$\vec{u}(l|n,\vec{q})=N^{-3/2}\sum_{s,j}a_{sj,n}(\vec{q})\exp[i\vec{q}_s\cdot\vec{x}(l)]\vec{e}(\vec{q}_s,j), \quad (17)$$

where $a_{sj,n}(\vec{q})$ is the coefficient of the $(n,\vec{q})$ mode expanded in terms of the bulk LO mode of $\vec{e}(\vec{q}_s,j)$. Here j is the polarization index ($j=1$, 2, and 3), $\vec{q}_s=\vec{q}+s\hat{Kz}$, $K=2\pi/d$ (the unit reciprocal lattice wave vector along the z direction), and s is an integer. Thus the Fröhlich electron-phonon interaction derived from this microscopic model can be written as[17]

$$H_{ep}(\vec{r})=\gamma V^{-1/2}\sum_{\vec{q},n}\omega_n^{-1/2}(\vec{q})\hat{a}^{+}_{n,\vec{q}}\times\sum_s a_{s,n}(\vec{q})e^{-i\vec{q}_s\cdot\vec{r}}/q_s+\text{c.c.}, \tag{18}$$

in which we have left out the polarization index j since the transverse bulk modes do not contribute to the potential.

III. ELECTRONIC SUBBAND STRUCTURES IN MQW's

In the present calculations, the electronic states in MQW's are treated within the effective-mass formalism. For simplicity, the hole is considered to be a simple particle, which differs from the electron only in the effective mass. Due to the different effective masses between the heavy and light holes, there are two series of hole subbands in the MQW's denoted by the heavy- and light-hole subbands, respectively. In the following, the formal notations for the electron and hole are often left out unless necessary.

The single-particle Hamiltonian can be written as

$$H(\vec{r})=-\frac{\hbar^2}{2m_W^*}\left(\frac{\partial^2}{\partial^2 x}+\frac{\partial^2}{\partial^2 y}\right)-\frac{\hbar^2}{2}\frac{\partial}{\partial z}\frac{1}{m^*(z)}\frac{\partial}{\partial z}+V(z), \tag{19}$$

where $m^*(z)$ was used to distinguish the electron mass in the well region, m_W^*, from that in barrier region, m_B^*; for holes, we simply take $m_W^*=m_B^*$. $V(z)$ is the MQW potential:

$$V(z)=V(z+nd)=\begin{cases}0, & |z|\leqslant d_0/2\\ V_0, & d_0/2\leqslant|z|\leqslant d/2.\end{cases} \tag{20}$$

The envelope function of the μth subband state can be expanded in terms of the bulk plane waves as:[32–33]

$$|\vec{k}_\parallel,\mu,k_z\rangle=\frac{1}{\sqrt{V}}e^{i\vec{k}_\parallel\cdot\vec{r}_\parallel}\sum_l c_{\mu,l}(k_z)e^{i(k_z+lK)z}, \tag{21}$$

where $c_{\mu,l}$ is the linear coefficient for the expansion, $(\vec{r}_\parallel,z)$ is the coordinate of the electron (or hole), and $(\vec{k}_\parallel,k_z)$ is the wave vector of the carrier.

The matrix element of the single Hamiltonian H between two plane waves can be written as

$$\langle k_z+l'K,\vec{k}'_\parallel|H|\vec{k}_\parallel,k_z+lK\rangle=\delta_{\vec{k}'_\parallel,\vec{k}_\parallel}\left(\left\{\frac{\hbar^2}{2m_W^*}k_\parallel^2+\frac{\hbar^2}{2m_+^*}(k_z+lK)^2+V_0\frac{d-d_0}{d}\right\}\delta_{l',l}+\left\{-V_0+\frac{\hbar^2}{2m_-^*}(k_z+lK)(k_z+l'K)\right\}\frac{\sin[(l-l')\pi d_0/d]}{(l-l')\pi}(1-\delta_{l',l})\right), \tag{22}$$

where $1/m_+^*=(d_0/d/m_W^*)+[(d-d_0)/d/m_B^*]$, and $1/m_-^*=1/m_W^*-1/m_B^*$. By solving the above secular equations, we can obtain the superlattice electron (hole) subband structure, i.e.,

$$E_n(\vec{k}_\parallel,k_z)=\frac{\hbar^2}{2m_W^*}k_\parallel^2+\epsilon_n(k_z), \tag{23}$$

and the corresponding coefficients $c_{\mu,l}(k_z)$ in Eq. (21), where n is the index for the electron (hole) subband.

IV. ENERGY-LOSS RATE FOR HOT CARRIERS IN MQW's

As the nondegeneracy statistics are not appropriate to the case of a high density of carriers at a relatively low carrier temperature, in this calculation the Fermi-Dirac distribution function is used to describe the distribution of the hot-carriers, i.e., $f(E)=1/(1+e^{(E-E_F)/k_BT})$, where E_F is the Fermi energy, which is determined by the carriers' type, density, and temperature.

According to Fermi golden rule, for a given phonon mode of $(n,\vec{q})$, the phonon generation rate $W_{n\vec{q}}$ by hot electrons or the hot holes can generally be expressed as

$$\begin{aligned}W_{n\vec{q}}=&\frac{2\pi}{\hbar}\sum_{n_i n_f\vec{k}}M(n_i,\vec{k}+\vec{q};n_f,\vec{k})\{(g_{n\vec{q}}+1)f(E_{n_i,\vec{k}+\vec{q}})[1-f(E_{n_f,\vec{k}})]-g_{n\vec{q}}\ f(E_{n_f,\vec{k}})[1-f(E_{n_i,\vec{k}+\vec{q}})]\}\\ &\times\delta(E_{n_i,\vec{k}+\vec{q}}-E_{n_f,\vec{k}}-\hbar\omega_{n\vec{q}})\\ =&\nu_{n\vec{q}}[g_{n\vec{q}}(T_c)-g_{n\vec{q}}],\end{aligned} \tag{24}$$

where $M(n_i,\vec{k}+\vec{q};n_f,\vec{k})$ stands for the square of the Fröhlich scattering matrix element between the electronic states of $(n_i,\vec{k}+\vec{q})$ and $(n_f,\vec{k})$, $E_{n_i,\vec{k}+\vec{q}}$ $(E_{n_f,\vec{k}})$ denotes the corresponding energy of the hot carrier at the initial (final) state as expressed by Eq. (23). $g_{n\vec{q}}(T)$ denotes the phonon occupation number at the temperature T, namely,

$$g_{n\vec{q}}(T)=1/(e^{\hbar\omega_{n\vec{q}}/k_BT}-1),$$

$g_{n\vec{q}}$ denotes the nonequilibrium phonon population, and

TABLE I. Parameters used for the calculations. m_0 is the mass of a free electron.

Symble	Meaning	Numerical value
a(GaAs)	lattice parameter of GaAs	5.653 Å
a(AlAs)	lattice parameter of AlAs	5.660 Å
m_e^*(GaAs)	electron effective mass of GaAs	$0.0665m_0$
m_e^*(AlAs)	electron effective mass of AlAs	$0.1495m_0$
γ_1	valence-band parameter of GaAs	6.85
γ_2	valence-band parameter of GaAs	2.10
ϵ_∞(GaAs)	high-frequency dielectric constant of GaAs	10.48
ϵ_∞(AlAs)	high-frequency dielectric constant of AlAs	8.16
ω_{LO}(GaAs)	LO-phonon frequency of GaAs	296.4 cm^{-1}
ω_{TO}(GaAs)	TO-phonon frequency of GaAs	273.1 cm^{-1}
ω_{LO}(AlAs)	LO-phonon frequency of AlAs	404.9 cm^{-1}
ω_{TO}(AlAs)	TO-phonon frequency of AlAs	363.5 cm^{-1}

$$\nu_{n\vec{q}}=\frac{2\pi}{\hbar}\sum_{n_i,n_f,\vec{k}} M(n_i,\vec{k}+\vec{q};n_f,\vec{k})\{f(E_{n_f,\vec{k}})-f(E_{n_i,\vec{k}+\vec{q}})\}\delta(E_{n_i,\vec{k}+\vec{q}}-E_{n_f,\vec{k}}-\hbar\omega_{n\vec{q}}), \tag{25}$$

The total generation rate for the mode $(n,\vec{q})$ is the summation of the phonon generation rate due to electrons $W^e_{n\vec{q}}$ and that due to holes $W^h_{n\vec{q}}$. Under the assumption that at each instant of relaxation process the net generation rate of phonon by hot carriers is equated to the phonon decay rate due to the anharmonic interaction, which is referred to as the quasistatic approximation, the nonequilibrium population for a given mode $(n\vec{q})$, $g_{n\vec{q}}$, is determined by

$$W^e_{n\vec{q}}+W^h_{n\vec{q}}=[g_{n\vec{q}}-g_{n\vec{q}}(T_L)]/\tau_0, \tag{26}$$

where τ_0 is the lifetime of the optical phonon due to the anharmonic interaction, which is assumed to be independent of the phonon mode and the phonon wave vector. Thus the hot-phonon population can be readily obtained from Eqs. (24) and (26):

$$g_{n\vec{q}}=\frac{\nu^e_{n\vec{q}}g_{n\vec{q}}(T_e)+\nu^h_{n\vec{q}}g_{n\vec{q}}(T_h)+g_{n\vec{q}}(T_L)/\tau_0}{\nu^e_{n\vec{q}}+\nu^h_{n\vec{q}}+1/\tau_0}, \tag{27}$$

where T_e represents the temperature of the hot electrons, and T_h is that of the hot holes which are considered identical in the following calculation.

Therefore, without the hot-phonon effect, the average energy loss rate per electron-hole pair is given by

$$P_0=\frac{1}{2\pi n_A N}\sum_{n,q_z}\int_0^\infty q_{||}\,dq_{||}\hbar\omega_{n\vec{q}}[\nu^e_{n\vec{q}}+\nu^h_{n\vec{q}}] \times[g_{n\vec{q}}(T_c)-g_{n\vec{q}}(T_L)]; \tag{28a}$$

and, with the hot-phonon effect, the average ELR is

$$P=\frac{1}{2\pi n_A N}\sum_{n,q_z}\int_0^\infty q_{||}\,dq_{||}\hbar\omega_{n\vec{q}}[\nu^e_{n\vec{q}}+\nu^h_{n\vec{q}}] \times[g_{n\vec{q}}(T_c)-g_{n\vec{q}}]. \tag{28b}$$

where n_A is the incident photon number per unit area, and the in-plane isotropy for hot phonons has been assumed. Note that if there is only one type of hot carrier (the electron gas or the hole gas) in the system investigated, only one term of $\nu_{n\vec{q}}$ is retained in the above expression, and accordingly P or P_0 is the average ELR per carrier.

V. RESULTS AND DISCUSSIONS

In our previous papers,[26,27] by using the microscopic dipole superlattice phonon model, we investigated in detail the hot-phonon population produced during the hot-electron and/or hot-hole relaxation in GaAs/AlAs MQW's. Since there is no essential difference between the ELR contributed by the electrons and that contributed by the holes within the simple effective-mass approximation, in this section we will concentrate on the phonon model effect on the ELR and the hot-phonon population contributed by the hot *electrons*.

In Table I we list the parameters used in the calculations, most of which are taken or derived from Ref. 34. The band-gap difference between GaAs and $Al_xGa_{1-x}As$ is taken to be $1.155x+0.37x^2$(eV), and the conduction-band offset between GaAs and $Al_xGa_{1-x}As$ is taken to be 60% of their band-gap difference. The average optical-phonon lifetime τ_0 is taken as 7 ps for all optical-phonon modes. The following calculations are carried out at a fixed carrier temperature of 100 K and at a lattice temperature of 10 K, with no other adjustable parameters used.

A. Nonequilibrium phonon population

The hot-phonon occupation number depends strongly on the phonon mode $(n\vec{q})$, because of the quite different matrix elements of electron-phonon coupling. In general, the value of the hot-phonon population is in the interval $g_{n\vec{q}}(T_L)$ and $g_{n\vec{q}}(T_c)$. In the following comparison of the hot-phonon population evaluated with different phonon models, a fixed

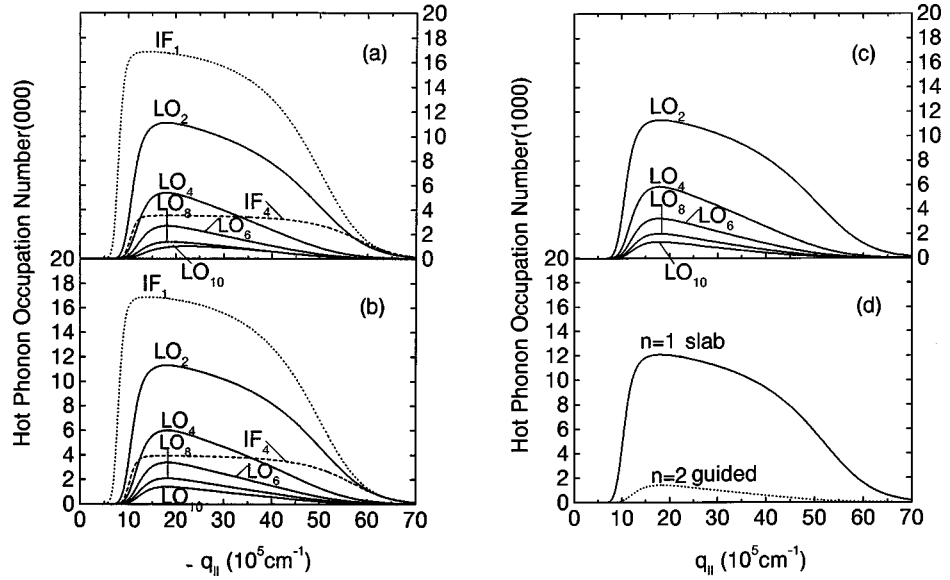

FIG. 1. The nonequilibrium phonon population from the electron relaxation as functions of $q_{||}$ for 10/10 MQW's calculated from (a) the microscopic model, (b) the original Huang-Zhu formulas, (c) the improved Huang-Zhu formulas, and (d) the slab model and the guided-mode model. The electron temperature and sheet density are $T=100$ K and $n_A=5.0\times10^{11}/\mathrm{cm}^2$, respectively. The nonequilibrium phonon population curves labeled with IF are for the interface modes.

sheet density of $5.0\times10^{11}/\mathrm{cm}^2$ of the hot electrons is considered, and the z-component of the phonon wave vector q_z is taken to be zero. In order to examine the effect of the well width on the hot-phonon population, we choose two MQW's with the well thickness of 10 and 50 monolayer (ML), respectively.

Figures 1 and 2 display the calculated hot-phonon occupation numbers in 10/10 [short for $(\mathrm{GaAs})_{10}(\mathrm{AlAs})_{10}$] and 50/50 MQW's, respectively. Figures 1(a), 2(a) and 2(e) represent results based on the microscopic dipole superlattice model with a vanishingly small bulk dispersion, while Figs. 1(b)–1(d), 2(b)–2(d), and 2(f) are the corresponding calculations with macroscopic models, in which all the bulklike modes are degenerate. In Figs. 1(b) and 2(b) the population of the bulklike modes based on the original Huang-Zhu analytical formulas are shown. The population curves for interface modes which are identical for both the dielectric continuum and Huang-Zhu models are also shown in Fig. 1(b), and shown separately in Fig. 2(f). Figures 1(c) and 2(c) represent the population of the bulklike modes calculated based on the improved Huang-Zhu analytical formulas; while the corresponding one in the slab model and that in the guided-mode model are shown in Figs. 1(d) and 2(d).

As shown in Figs. 1 and 2, the calculated nonequilibrium phonon numbers vary strongly with the transverse wave number $q_{||}$. Because of the requirements of conservation of both energy and transverse momentum, the most probable hot optical phonons produced in thin wells are located within a region around the parallel wave number of $[2m^*\omega_{LO}/\hbar]^{1/2}$, while the occupation number of the modes with $q_{||}$ out of the region are several orders of magnitude smaller except for the case where the resonant intersubband scattering is available.

The confined bulklike modes and the interface modes with zero q_z in the macroscopic models have definite parity. As the intrasubband relaxation $(1\rightarrow1)$ dominates in thin quantum wells, in Figs. 1(b)–1(d) only modes associated with the potential function of even parity with respect to the well center appear. When the well becomes wider, the intersubband electron-phonon scattering become more and more important. Since the parities of the neighboring electronic subbands are opposite, as illustrated in Fig. 2, in addition to the even modes a hot-phonon population for confined modes with odd parity appears.

In Fig. 1, both the original and improved Huang-Zhu formulas give almost identical phonon occupation numbers with that from the microscopic model. As shown in Figs. 2(a)–2(c), the improved Huang-Zhu model and the microscopic model lead to quite similar results for the population of the confined modes; however, the agreement between the original and improved Huang-Zhu formulas deteriorates when the mode index or the parallel wave number increases, because the original Huang-Zhu analytical formula are orthogonal only when $q_{||}$ is not large compared with π/W_0.

Unlike the microscopic model and the Huang-Zhu model, in which all modes with proper symmetries participate in the hot-carrier relaxation process (though the occupation number decreases significantly with an increase of the mode order index), in MQW's with thin wells [Fig. 1(d)] only the $n=1$ mode in the slab model and the $n=2$ confined mode in the guided-mode model are generated significantly during the relaxation process of the hot electrons, in addition to the interface modes in the dielectric model. Other modes' contributions are 2–3 orders of magnitude smaller than that of the lowest allowed mode. When the well width increases [Fig. 2(d)], or when the contributions from the hot holes is taken into account, several lower bulklike modes may make contributions to the intersubband and higher intrasubband scattering.

It needs pointing out that the hot-phonon occupation number calculated with the guided-mode model is significantly smaller than that in other models, because (1) the interface modes are absent from the guided-mode model, and (2) the lowest even-mode potential in this model has the form of

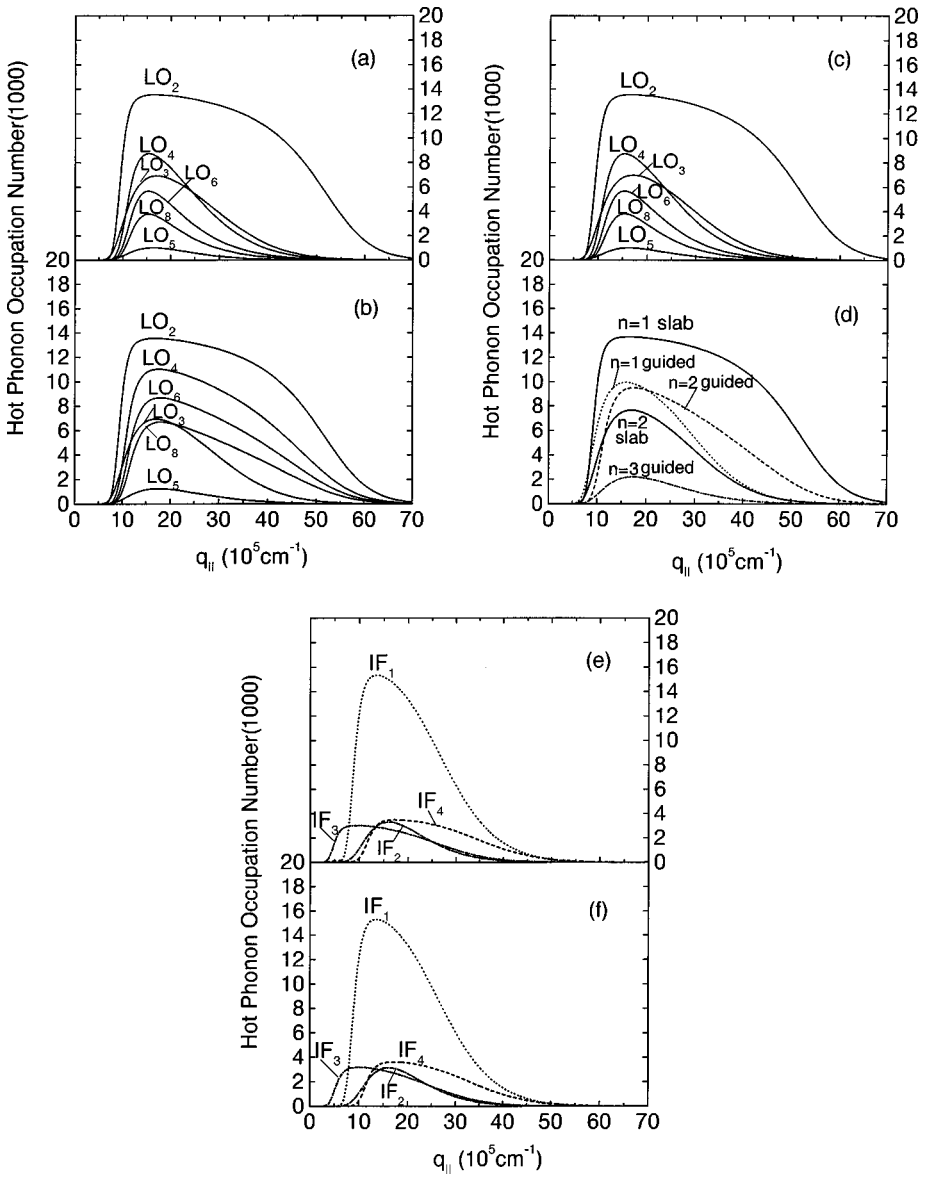

FIG. 2. The calculation for the $q_{||}$ dependence of nonequilibrium phonon population emitted in the hot-electron relaxation process in 50/50 MQW's. All the notations and illustrations are similar to Fig. 1 except that the population for interface modes is respectively shown in (e) (the microscopic model) and (f) (the macroscopic model).

$\cos(2\pi z/W)$, which has negative antinodes at the interfaces and a positive maximum value at the well center, leading to a largely canceled overlap integral in the interaction matrix element.

As regards the nonequilibrium phonon population contributed by the interface modes, there is little difference between the macroscopic and the microscopic phonon models. The interface modes are associated with a definite parity for zero q_z in the macroscopic models, thus in Fig. 1(b) only the symmetric interface modes of GaAs and AlAs are emitted in the intrasubband relaxation. In the microscopic calculation, the interface mode potential does not manifest itself in a definite parity, even when $q_z \rightarrow 0$. However, as shown in Figs. 1(a)and 2(e), if we linearly combine the pair of nearly degenerate interface modes, the obtained hot-phonon population is not significantly different from that in the macroscopic models.

When taking a close look at Figs. 1 and 2, we have found that, with increasing well width, the hot-phonon populations of the bulklike modes are enhanced at the expense of the reduced population of the interface modes. This reflects the fact that the potentials accompanying the interface modes decay exponentially when moving away from the interfaces, and thus lead to decreased electron–interface-mode coupling in wide wells.

Another point we should mention concerns comparing the occupation numbers of the GaAs- and AlAs-like interface modes. The fact that the population of GaAs-like interface modes is significantly larger than that of the AlAs-like interface modes does not imply that the matrix element between the electron states and the GaAs-like interface modes is stronger than the AlAs-like one; on the contrary, the latter is stronger than the former in a thin well. This is owing to the fact that the upper limit for the hot-phonon population of the GaAs-like interface modes, $g_{IF}(GaAs,T_c)$, is much larger than that of the AlAs-like modes, as $\omega_{IF}(AlAs)$ is higher than $\omega_{IF}(GaAs)$.

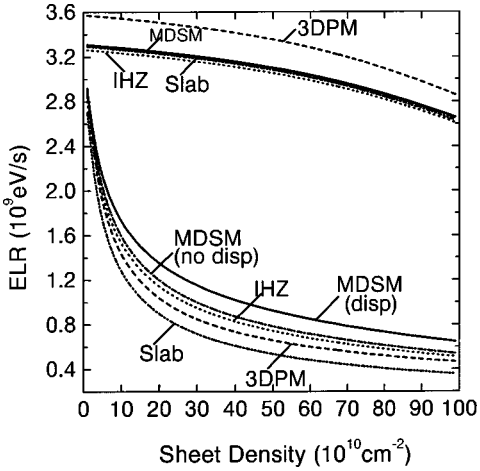

FIG. 3. Comparison between the electron ELR's as functions of sheet density in 35/35 MQW's ($T=100$ K) calculated with different phonon models, including the improved Huang-Zhu model (IHZ), the slab model (Slab), the three-dimensional phonon model (3DPM), and the microscopic model with [MDSM(disp)] and without [MDSM(no disp)] bulk-phonon dispersion. Within the two curves labeled with same phonon model, the lower (upper) curve represents the calculated ELR with the hot-phonon effect included (excluded). disp stands for including the bulk-phonon dispersion.

B. Energy-loss rate of hot electrons

Figure 3 shows the sheet density dependence of the electron ELR's in the 35/35 MQW's evaluated by various analytical phonon models as well as the microscopic model. Because the ELR calculated with the guided-mode model is several times less than the results of other models, the data will be omitted. Since the improved Huang-Zhu formulas are more exact than the original one, the ELR's calculated with the original Huang-Zhu formulas will not be shown here either. In the following, results calculated with the improved Huang-Zhu formulas will be referred to simply as results from the Huang-Zhu model, if not specifically denoted. For the sake of comparison, two groups of curves are drawn in Fig. 3, in which the upper group is the calculated ELR's without the hot-phonon effect, and the lower group is the corresponding one with the hot-phonon effect. Each curve is labeled by the phonon model used.

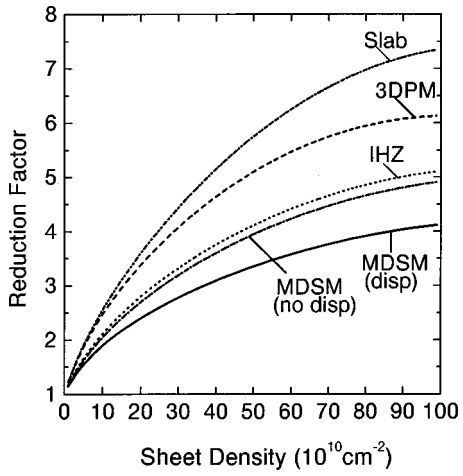

FIG. 4. The hot-phonon reduction factors for electron ELR's as functions of the sheet density in 35/35 MQW's ($T=100$ K) calculated based on the various phonon models: the slab model, the three-dimensional phonon model (3DPM), the improved Huang-Zhu model (IHZ), and the microscopic phonon model with [MDSM (disp)] and without [MDSM(no disp)] bulk-phonon dispersion.

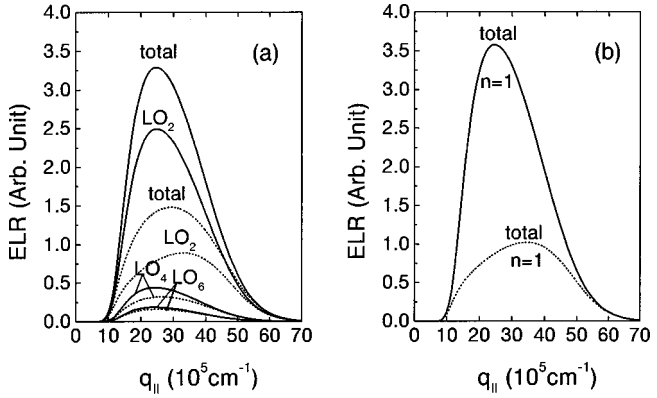

FIG. 5. Comparison of the electron differential ELR's by various confined modes calculated with (a) the improved Huang-Zhu model and (b) the slab model, as functions of the parallel wave number $q_{||}$ in 10/10 MQW's ($T_c=100$ K, and the volume density is 1.0×10^{18} cm^{-3}). Total denotes the differential ELR contributed from all the confined modes, but, in slab model (b), the total contribution and the contribution from the lowest order of modes ($n=1$) coincide. Solid lines: hot-phonon effect excluded; dotted lines: hot-phonon effect included.

Without the hot-phonon effect, ELR's as functions of the electron density calculated by the Huang-Zhu model, the slab model and the microscopic model (whether the bulk-phonon dispersion is included or not), respectively, are very close. The only exception is the ELR's calculated with the three-dimensional phonon model, which are a little larger compared to others. When the electron density is as high as 10^{12}/cm^2, the finite probability occupied by final electronic states obviously reduces the ELR's. Our calculation indicates that if the ELR's contributed the confined modes and the interface modes are evaluated separately, the carrier degeneracy effect mainly affects the ELR's through the confined modes, and only slightly affects the ELR's by the interface modes owing to their dispersive character.

When including the hot-phonon effect, with the sheet density of carrier increased, the hot-phonon effect reduces the ELR's of electrons substantially, and the different phonon models do give different ELR's. As shown in Fig. 3, the Huang-Zhu model and the microscopic model without the bulk-phonon dispersion give roughly the same ELR's, which are significantly faster than those based on the three-dimensional phonon model and the slab model, but slower than the results based on the microscopic model with the bulk-phonon dispersion.

To measure the hot-phonon effect, we introduce the hot-phonon reduction factor α, which is defined as the ratio of the ELR without the hot-phonon effect over those with the hot-phonon effect, namely, $\alpha=P_0/P$, where P and P_0 are the expressions of Eqs. (28b) and (28a). The reduction factors for electron ELR's given by different phonon models as functions of the sheet density are shown in Fig. 4. It is evident that the hot-phonon effect on the ELR is sensitive to the

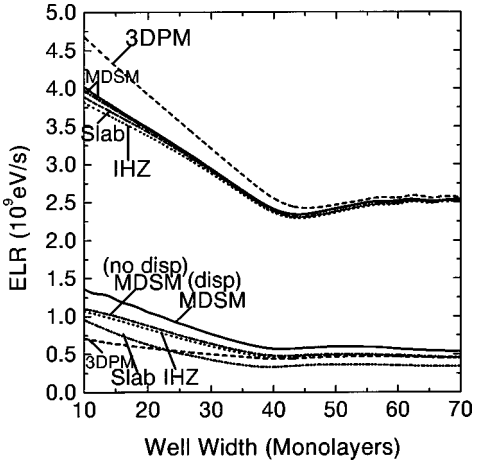

FIG. 6. Electron ELR's as functions of the well widths, calculated by using different phonon models ($T=100$ K, $n_V=1.0\times10^{18}$ cm^{-3}). The labels for the phonon models are the same as in Figs. 3 and 4. The upper (lower) group of curves stands for ELR's without (with) the hot-phonon effect, respectively. disp denotes that the bulk-phonon dispersion is considered in the microscopic model.

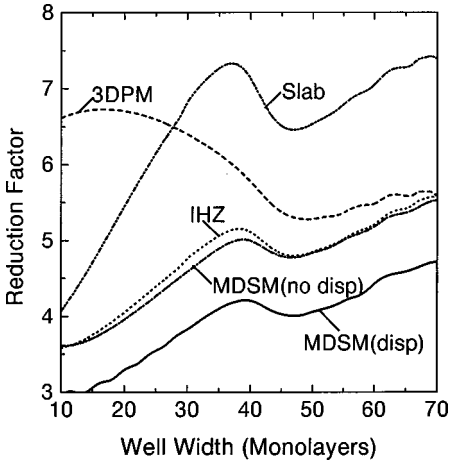

FIG. 7. The phonon model dependence of the hot-phonon reduction factors as functions of the well width for electrons at $T=100$ K, and with a volume density of 1.0×10^{18} cm^{-3}. The labels for the phonon models are the same as in Figs. 3 and 4.

phonon models adopted. Among all these models shown in Fig. 4, the slab model overestimates the hot-phonon effect most as compared to the microscopic model.

Why are ELR's calculated based on the slab model significantly slower than those calculated based on the Huang-Zhu model when the hot-phonon effect is included, while they are almost identical without the hot-phonon effect? Since the interface modes are identical in both models, we will only examine the behaviors of the bulklike modes. As an example let us take an electron gas with a volume density of 1.0×10^{18} cm^{-3} in the 10/10 MQW's [Figs. 5(a)–5(b)]. In the slab model, the confined phonons emitted in the electron relaxation process concentrate to a lowest order of $n=1$, while for the Huang-Zhu model all the confined phonon modes with even parity take part in the relaxation process. The hot phonons in the slab model ($n=1$ mode), being part of the strongest coupling matrix elements, are hotter than the hot-phonon modes in the Huang-Zhu model; however, the nonequilibrium phonon population of the $n=1$ mode in the slab model, being restricted by $g(T_c)$, is less than the sum of the nonequilibrium phonon population of all the confined $n=even$ modes in the Huang-Zhu model, which is responsible for the larger hot-phonon reduction factors in the slab model.

In order to investigate the influence of well width on the electron relaxation, we have calculated the well-width dependence of ELR's in MQW's with equal well and barrier width by using several macroscopic and microscopic phonon models. In the calculations, the concentration of the hot electrons is fixed to be 1.0×10^{18} cm^{-3}. In Fig. 6, two groups of curves stand for ELR's without and with the hot-phonon effect, respectively. Some interesting results can be seen from Fig. 6.

First, in agreement with our very recent paper,[35] when the hot-phonon effect is considered, among several macroscopic phonon models the Huang-Zhu model gives cooling rates of hot electrons that are closest to the microscopic model with the dispersionless bulk phonon, but significantly slower than ELR's calculated with the microscopic model with the dispersive bulk phonon, although it exhibits no influence on ELR's without the hot-phonon effect whether the bulk phonon is dispersive or not.

Second, for MQW's with thin wells and barriers, when the hot-phonon effect is not considered, ELR's based on various macroscopic phonon models are not exactly in agreement, and deviate from the results of the microscopic models. The possible reasons for this might be (1) the coupling effect due to the thin barrier on the phonon potential which is accounted for in the microscopic model but ignored in the macroscopic models, and (2) the incompleteness of the basis set in the thin well.

Third, for a well width of less than 45 ML, all phonon models predict that the ELR's of hot electrons decrease with increasing well width. This arises from the facts that when the well width iincreases, the electron–interface-phonon scattering decreases, and the degeneracy effect is enhanced because the sheet density increases with the well width for a

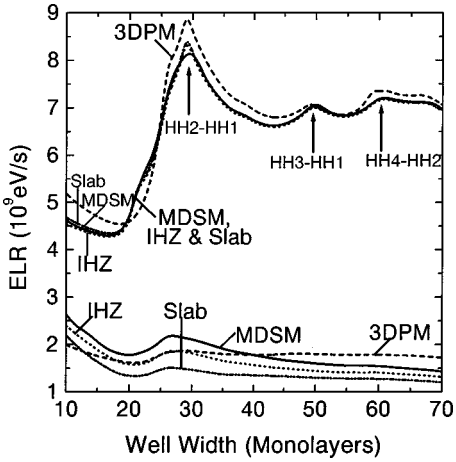

FIG. 8. Well-width dependence of hole ELR's obtained from different phonon models ($T=100$ K, $n_V=1.0\times10^{18}$ cm^{-3}). The subbands involved in the resonant intersubband scattering are labeled near the peak in the curves. The notations labeled for the phonon models are the same as in Figs. 3 and 4.

fixed volume density. For a well width larger than 45 ML, the ELR tends to increase slightly as the intersubband scattering strengthens.

Fourth, the cooling rates estimated by the three-dimensional phonon model are good for a wide well, but the error increase notably as the well becomes thinner.

The hot-phonon reduction factors for electron ELR's as functions of the well width, calculated from several phonon models, are displayed in Fig. 7. It is seen that when the well thickness is less than about 40 ML, the hot-phonon effect on the electron relaxation is expected to enhance with the well width for a fixed volume density, with the three-dimensional phonon model the only exception. Both the three-dimensional phonon model and the slab model overestimate the hot-phonon effect compared to the microscopic model. The slab model gives a hot-phonon reduction factor α about 40% greater than that given by the improved Huang-Zhu model, and about 75% percent greater compared with the microscopic model with the dispersive bulk phonons.

Figure 8 shows the hole ELR's calculated from the Huang-Zhu model, the slab model, and the microscopic model (dispersive bulk phonon) as functions of the well width, in which the hole temperature and volume density are fixed at 100 K and 1.0×10^{18} cm^{-3}, respectively. The results show that without the hot-phonon effect, the hole ELR reaches a maximum value at a certain well width, which arises from the resonant intersubband scattering when the separation between two hole subbands is equal to the optical-phonon energy. The two subbands involved in the resonant transition are labeled near the corresponding peak in Fig. 8. Similar to the case for hot electrons, when ignoring the hot-phonon effect the phonon models give nearly equal ELR's; however, when the hot-phonon effect is taken into account, the slab model overestimates the hot-phonon effect on the hole relaxation compared to the microscopic model. In addition, owing to the larger density of states for holes, the degeneracy effect on the ELR's of holes is not important, and thus the hole ELR varies little with the well width for wide MQW's.

VI. CONCLUSIONS

In conclusion, we have calculated the carrier energy-loss rate in multiple quantum wells by using four analytical phonon models and the microscopic dipole superlattice model. It is found that when the hot-phonon effect is taken into account, the ELR is noticeably dependent on the phonon models used, though insensitive to the phonon models without the hot-phonon effect except for the guided-mode model. Out of the macroscopic phonon models investigated, the improved Huang-Zhu model presents the results closest to the microscopic model: it is roughly the same as the microscopic model when the bulk phonons are assumed to be dispersionless, and deviates somewhat from the microscopic model when the phonon dispersion is fully considered. The slab model and the three-dimensional phonon model overestimate the hot-phonon effect on the hot-carrier relaxation compared with the microscopic model without bulk-phonon dispersion, and deviate furthermore from the microscopic model with a dispersive bulk phonon. Owing to the fact that the formulas given by Huang and Zhu are not strictly orthogonal, Nash's improvement is necessary for quantitatively evaluating the carrier ELR's in wide quantum wells.

ACKNOWLEDGMENTS

We wish to acknowledge support from the National Natural Science Foundation of China, and the Qiu-Shi Science and Technology Foundation in Hong Kong.

*Present address: State Key Laboratory for Surface Physics, Institute of Physics, Chinese Academy of Sciences. P.O. Box 603, Beijing 100080, P.R. China.

[1] K. T. Tsen, R. P. Joshi, D. K. Ferry, and H. Morkoc, Phys. Rev. B **39**, 1446 (1989).
[2] J. Shah, R. C. C. Leite, and J. F. Scott, Solid State Commun. **8**, 1089 (1970).
[3] J. Shah, *Ultrafast Spectroscopy of Semiconductors and Semiconductor Nanostructures*, Springer Series in Solid State Science Vol. 115 (Springer-Verlag, Berlin, 1996).
[4] P. J. Price, Physica B **134**, 164 (1985).
[5] P. Lugli and S. M. Goodnick, Phys. Rev. Lett. **59**, 716 (1987).
[6] W. Cai, M. C. Marchetti, and M. Lax, Phys. Rev. B **35**, 1369 (1987).
[7] J. Shah, A. Pinczuk, A. C. Gossard, and W. Wiegmann, Phys. Rev. Lett. **54**, 2045 (1985).
[8] K. Leo, W. W. Rühle, and K. Ploog, Phys. Rev. B **38**, 1947 (1988).
[9] K. J. Nash, Phys. Rev. B **46**, 7723 (1992).
[10] H. Rucker, E. Molinari, and P. Lugli, Phys. Rev. B **45**, 6747 (1992).
[11] I. Lee, S. M. Goodnick, M. Gulia, E. Molinari, and P. Lugli, Phys. Rev. B **51**, 7046 (1995).
[12] N. Mori and T. Ando, Phys. Rev. B **40**, 6175 (1989).
[13] L. F. Register, Phys. Rev. B **45**, 8756 (1992).
[14] R. Fuchs and X. Kliewer, Phys. Rev. A **140**, A2076 (1965).
[15] M. Barbiker, J. Phys. C **19**, 683 (1986).
[16] B. K. Ridley, Phys. Rev. B **39**, 5282 (1989).
[17] Kun Huang and Bang-fen Zhu, Phys. Rev. B **38**, 13 377 (1988).
[18] Kun Huang and Bang-fen Zhu, Phys. Rev. B **38**, 2183 (1988).
[19] Bang-fen Zhu, Phys. Rev. B **38**, 7694 (1988).
[20] In the literature, the ''Huang-Zhu model'' usually refers to the simple analytical simulations of the polar-optical-phonon modes in MQW's and the double boundary condition. In much rarer cases, the Huang-Zhu model has been used to designate the dipole oscillator superlattice model. In our work, we have found that it serves as a relatively simple and fairly satisfactory microscopic model for the optical vibration in superlattices.
[21] K. T. Tsen, Keith R. Wald, Tobias Ruf, Peter Y. Yu, and H. Morkoc, Phys. Rev. Lett. **67**, 2557 (1991).
[22] G. Weber, A.M. de Paula, and J. F. Ryan, Semicond. Sci. Technol. **6**, 397 (1991).
[23] S. Rudin and T. L. Reinecke, Phys. Rev. B **41**, 7713 (1990).
[24] Bang-fen Zhu, Phys. Rev. B **46**, 13 619 (1992).
[25] K. J. Nash and D. J. Mowbray, J. Lumin. **44**, 315 (1989).
[26] Bang-fen Zhu, Kun Huang, and Jian-zhong Zhang, Superlattices Microstruct. **23**, 87 (1998).
[27] Bang-fen Zhu, Jian-zhong Zhang, and Kun Huang (unpublished).
[28] B. K. Ridley, *Electrons and Phonons in Semiconductor Multilayers* (Cambridge University Press, Cambridge, 1997).

[29] E. Molinari, A. Fasolino, and K. Kunc, Phys. Rev. Lett. **56**, 1751 (1986); A. K. Sood, J. Menendez, M. Cardona, and K. Ploog, *ibid.* **56**, 1753 (1986).

[30] G. Weber pointed out that the slab model is not a complete basis and proposed another set of reformulated slab model [Phys. Rev. B **46**, 16 171 (1992)]. In fact, as pointed out by Nash, in both slab and Huang-Zhu model, the completeness can be realized only by combining both the bulklike and interface modes.

[31] Kun Huang, Bang-fen Zhu, and Hui Tang, Phys. Rev. B **41**, 5825 (1990).

[32] Bang-fen Zhu and Y. C. Chang, Phys. Rev. B **50**, 11 932 (1994).

[33] H. Tang and K. Huang, Chin. Phys. **8**, 1101 (1987).

[34] *Semiconductors. Physics of Group IV Elements and III-V compounds*, edited by O. Madelung, M. Schulz and H. Weiss, Landolt-Börnstein, New Series, Group III, Vol. 17, Pt. a (Springer-Verlag, Berlin, 1982).

[35] Bang-fen Zhu, Jian-zhong Zhang, and Kun Huang, in *Proceedings of the 24th International Conference on the Physics of Semiconductors*, edited by D. Gershoni (World Scientific, Singapore, 1999).